

Interpretable Deep Learning for Probabilistic MJO Prediction

Antoine Delaunay¹ and Hannah M. Christensen²

¹Department of Applied Mathematics, Ecole Polytechnique, Palaiseau, France

²Department of Physics, University of Oxford, Oxford, UK

Key Points:

- A deep convolutional neural network (CNN) is used to produce probabilistic forecasts of the MJO
- The forecasts provide well-calibrated state-dependent estimates of forecast uncertainty
- The CNN forecasts are used to probe sources of predictability for the MJO

Corresponding author: Hannah M. Christensen, hannah.christensen@physics.ox.ac.uk

Abstract

The Madden–Julian Oscillation (MJO) is the dominant source of sub-seasonal variability in the tropics. It consists of an Eastward moving region of enhanced convection coupled to changes in zonal winds. It is not possible to predict the precise evolution of the MJO, so subseasonal forecasts are generally probabilistic. Ideally the spread of the forecast probability distribution would vary from day to day depending on the instantaneous predictability of the MJO. Operational subseasonal forecasting models do not have this property. We present a deep convolutional neural network that produces skilful state-dependent probabilistic MJO forecasts. This statistical model accounts for intrinsic chaotic uncertainty by predicting the standard deviation about the mean, and model uncertainty using a Monte-Carlo dropout approach. Interpretation of the mean forecasts from the neural network highlights known MJO mechanisms, providing confidence in the model, while interpretation of the predicted uncertainty indicates new physical mechanisms governing MJO predictability.

Plain Language Summary

The Madden–Julian Oscillation (MJO) is an important tropical climate phenomenon. It consists of enhanced convective thunderstorms and anomalous winds that propagate eastward along the Equator for a few weeks. The MJO is difficult to predict and exhibits great variability. This means that forecasts are often probabilistic. However, current models have difficulty in correctly predicting the uncertainty in the forecast based on the current conditions. In this paper, we propose a model using neural networks capable of making reliable probabilistic forecasts. We interpret the behaviour of the algorithm to verify its consistency with the known physical mechanisms of the MJO and to highlight new physical conditions that affect MJO prediction uncertainty.

1 Introduction

The Madden-Julian Oscillation (MJO: Madden & Julian, 1971) is an envelope of enhanced tropical convection with associated changes to the atmospheric circulation. It is characterised by its period of 40-50 days, its planetary scale, and its Eastward propagation at speeds of 4–8 ms^{-1} . It is the major source of predictability on sub-seasonal timescales in the Tropics (Zhang, 2013) and influences phenomena such as the North Atlantic Oscillation and Arctic sea ice cover through global teleconnections (Ferranti et al.,

1990; Cassou, 2008; Yoo et al., 2012; Henderson et al., 2014). Subseasonal forecasts are of great socio-economic value through their potential to predict extreme weather events several weeks ahead (Vitart & Robertson, 2018). There is therefore great interest in improving predictions of the MJO, and in understanding sources of MJO predictability (Kim et al., 2018).

The chaotic nature of the Earth System means that it is not possible to predict the precise evolution of the MJO beyond a few days, so subseasonal forecasts are generally probabilistic (J. Slingo & Palmer, 2011; Bauer et al., 2015). If the probabilistic forecast *mean* is assessed, averaging out the unpredictable ‘noise’, current dynamical models have a prediction skill up to three weeks (Lim et al., 2018; Vitart, 2017). However, systematic biases remain, especially in the propagation of the MJO convective anomaly over the Maritime Continent (Kim et al., 2016; Barrett et al., 2021; Li et al., n.d.). In contrast to the mean skill, the *probabilistic* skill of MJO forecasts is low (Lim et al., 2018; Vitart, 2017). Improving probabilistic forecasts is essential to quantify our confidence in the predictions, and to advance understanding of the predictability of this phenomenon.

While prediction skill is a property of the forecast model, predictability is a property of the Earth-system. MJO predictability studies have focused on the theoretically achievable prediction limit that one could achieve with a perfect model, quantified as 6–7 weeks (e.g. Neena et al., 2014; Wu et al., 2016; Kim et al., 2018). This is complementary to an approach taken in the medium-range forecasting community, where ‘predictable’ forecasts are those for which the forecast uncertainty is small (e.g. Palmer, 2000). This identification is possible because medium-range forecasts exhibit state-dependent reliability (Leutbecher & Palmer, 2008). If reliable, state-dependent, MJO forecasts could be produced, forecast uncertainty could be used as an indicator of instantaneous MJO predictability.

Increasing volumes of data, advances in computational power, and developments in statistical modelling have led to substantial interest in the use of machine learning in Earth-system science (Reichstein et al., 2019; Huntingford et al., 2019). Deep learning has been applied to the MJO for phase classification (Toms et al., 2020; Martin et al., 2021), post processing (Kim et al., 2021), and deterministic prediction (Martin et al., 2021). Here, we develop a neural network that produces well calibrated probabilistic forecasts of the MJO. We use a convolutional neural network (CNN), which has proved

75 effective at identifying hidden patterns and processes in climate (Ham et al., 2019; Ar-
76 comano et al., 2020; Schultz et al., 2021) and other scientific areas such as image recog-
77 nition (Russakovsky et al., 2015).

78 The paper is structured as follows: in Section 2, we describe the CNN, including
79 the data used to train the model. In Section 3 we present our results. We evaluate the
80 CNN compared to dynamical models from the Subseasonal-to-Seasonal prediction project.
81 We validate the CNN by seeking to understand its mean forecasts, before using the CNN
82 to uncover potential sources of predictability for the MJO. Finally we discuss the sig-
83 nificance of our results and draw conclusions in Section 4.

84 **2 Methods**

85 **2.1 Data**

86 Observational data used to train and test the CNN are taken from the ECMWF
87 Reanalysis version 5 (ERA5) dataset between 1979–2019 (Hersbach, H., et al., 2020). We
88 compare the CNN to models from the Subseasonal-to-Seasonal (S2S) prediction project
89 database (F. Vitart et al., 2017). We select reforecast data from four representative mod-
90 els, chosen to span the range of performances of models in the S2S database. In partic-
91 ular, we include the European Centre for Medium-Range Weather Forecasts (ECMWF)
92 model, which is known to produce the most skilful MJO forecasts (Lim et al., 2018). The
93 remaining models chosen had the largest reforecast ensemble size, enabling probabilis-
94 tic forecast skill to be assessed. Further details are presented in Supporting Table 1.

95 **2.2 Overview of Predictive Model**

96 The MJO is a coupled convective-dynamic anomaly that can be summarised by the
97 bivariate Real-time Multivariate MJO (RMM) index (Wheeler & Hendon, 2004). The
98 RMM index classifies active MJO events (amplitude greater than one) into one of eight
99 phases depending on geographical location (e.g. Supporting Figure S1). Using observed
100 daily-mean input maps at a single date t , we train a deep CNN to predict RMM1 and
101 RMM2 at a later date $t + \tau$, training a separate CNN for each lead time. The chosen
102 lead times are one, three and five days, then every fifth day up to 35 days. The archi-
103 tecture of the CNN is shown in Supporting Figure S2.

104 We compute the observed values of the RMM following Wheeler and Hendon (2004)
105 (see Supporting Information Text S1 for details). Subseasonal anomalies of Outgoing Long-
106 wave Radiation (OLR) and zonal wind at 200 hPa (UA200) and 850 hPa (UA850) be-
107 tween 20°S–20°N are latitudinally averaged and divided by their global variance. The
108 first two Empirical Orthogonal Functions (EOFs) of the combined fields are computed.
109 RMM1 and RMM2 are the projection of the daily fields onto EOFs 1 and 2.

110 Even though the MJO shows seasonal behaviour, we train a single model for all
111 seasons to maximise the available training data. As inputs we use subseasonal anoma-
112 lies of OLR, UA200, and UA850, consistent with fields used to compute the RMM in-
113 dices. We supplement these with four further fields which provide complementary infor-
114 mation: daily mean Specific Humidity at 400 hPa (SHUM400) was included because Barrett
115 et al. (2021) reported large differences in SHUM400 between MJO events which prop-
116 agate and weaken over the Maritime Continent; daily mean geopotential at 850 hPa (Z850)
117 provided skill in previous work (Toms et al., 2020); daily mean Downwelling Longwave
118 Radiation at the surface (DLR) has a marked annual cycle, which we found a more ef-
119 fective means of accounting for the seasonality of the MJO than including a dummy vari-
120 able. Finally, daily anomalies of sea surface temperature (SST) are included, since the
121 MJO is known to be linked to El Nino-Southern Oscillation (ENSO: e.g. Kessler, 2001).
122 Inputs are provided as maps spanning 0–360°E, 20°S–20°N on a 2.5°x2.5° grid. The dif-
123 ferent variables are input to the CNN as separate channels. This allows the CNN to learn
124 to identify co-located phenomena. To ensure independence between the training and test-
125 ing data sets, we use the first 80% of the dates for training, and the remaining 20% for
126 testing.

127 We model the two forecast RMM indices as following a Gaussian Bivariate distri-
128 bution with null correlation (Wheeler & Hendon, 2004). The network outputs the pre-
129 dicted means and variances of RMM1 and RMM2, and is trained by minimising the neg-
130 ative log-likelihood. The output variance represents the intrinsic chaotic (aleatoric) un-
131 certainty in the prediction. In addition, we represent the epistemic uncertainty in the
132 CNN model weights using a Monte-Carlo Dropout method to produce an ensemble of
133 forecasts (Gal & Ghahramani, 2016; Gal, 2016; Scalia et al., 2019). The total forecast
134 uncertainty is the sum of the aleatoric and epistemic variances. More details are provided
135 in Supporting Information Text S2.

2.3 Interpretation using PatternNet

We use the PatternNet algorithm (Kindermans et al., 2017) to interpret forecasts made by the CNN, as it outperforms other approaches including Guided BackProp and Layerwise Relevance Propagation in both idealised test cases and for image classification problems (Kindermans et al., 2017). Inputs to the CNN include a *signal*, that contains information about the future state of the MJO, and a *distractor*. PatternNet is a distinct network to the CNN, but whose structure reflects that of the CNN in reverse, propagating the estimated signal from the output to the input space, thereby disentangling the signal from the distractor: for more details, see Supporting Information Text S4.

3 Results

3.1 Network performance

Figure 1 compares the network’s performance to models from the S2S database (see Supporting Information Text S5 for definitions of all metrics). Figures 1(a–c) show the deterministic skill of the CNN mean forecasts in terms of the Root Mean Square Error (RMSE), Amplitude Error, and Phase Error respectively. In terms of RMSE, the CNN is competitive with models from the S2S database, though has larger errors than ECMWF. Similarly to the dynamical models, the CNN forecasts suffer from an increasing amplitude error with time, indicating a decay in MJO strength over the duration of the forecast. It is known that dynamical models simulate slower MJO propagation speeds than observed, resulting in a negative phase error. Here the CNN outperforms the dynamical models, accurately capturing the MJO propagation speed.

Figures 1(d–f) assess the probabilistic skill of the CNN forecast. The Continuous Ranked Probability Score (CRPS: Marshall et al. (2016)) compares the forecast and observed cumulative distribution functions. The CNN is competitive with forecast from the S2S database, outperforming three of the four dynamical models considered. Despite being widely used, the CRPS can give unintuitive rankings (e.g Bolin & Wallin, 2019), as it more severely penalises errors in the forecast mean than poor calibration of spread (Christensen et al., 2015). An alternative score is the ‘Ignorance’ or log-score (Roulston & Smith, 2002), shown in Panel (e). This score is local, derived from information theory, and easily generalises to multivariate predictions (Roulston & Smith, 2002; Bjerregård et al., 2021).

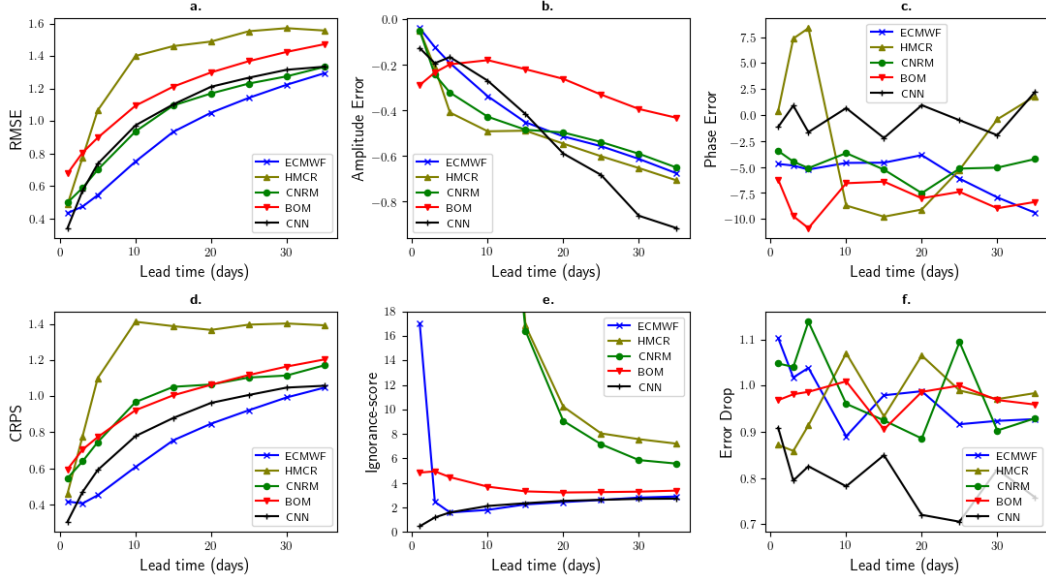


Figure 1. Skill of CNN (black), compared to forecasts from the subseasonal-to-seasonal prediction project (colours) as a function of lead time. (a) Root mean square error. (b) Amplitude error. (c) Phase error. (d) Continuous Ranked Probability Score. (e) Log-score (also known as the Ignorance Score). CNRM and HMCR scores before day-15 were too high to be shown. (f) Error-Drop. For all scores, a value closer to zero indicates a more skilful forecast.

167 It is also consistent with the loss function used to train the network. According to the
 168 log-score, the CNN is one of the two models with the best forecast skill at lead times of
 169 5–35 days. At shorter lead times, it outperforms all dynamical models. The poor per-
 170 formance of dynamical models at these short lead times is due to overconfident forecasts
 171 (Bjerregård et al., 2021), which are penalised by the log-score. In contrast, the CNN is
 172 able to balance the loss in accuracy with an increasing predicted uncertainty as the lead
 173 time increases.

174 For probabilistic forecasts to be useful, observations should behave as if they were
 175 drawn from the forecast probability distribution. For this to hold, a smaller forecast spread
 176 should indicate a smaller root mean squared error (RMSE) in the forecast mean on aver-
 177 age. We assess this property of the forecasts using Error-Spread diagrams (Leutbecher
 178 & Palmer, 2008) shown in Figure 2. For well calibrated forecasts, the observed RMSE
 179 should equal the predicted standard deviation, with scattered points lying on the one-
 180 to-one line. None of the dynamical models have this property: their error distributions
 181 are independent of the forecast spread, such that the spread gives no indication of the

182 true predictability of the MJO on that day. In contrast, if the CNN forecast spread is
 183 low, the RMSE is indeed smaller than if the spread is high. The probabilistic forecasts
 184 produced by the CNN are a dynamic indicator of the certainty in the MJO forecasts, and
 185 therefore the instantaneous predictability of the MJO.

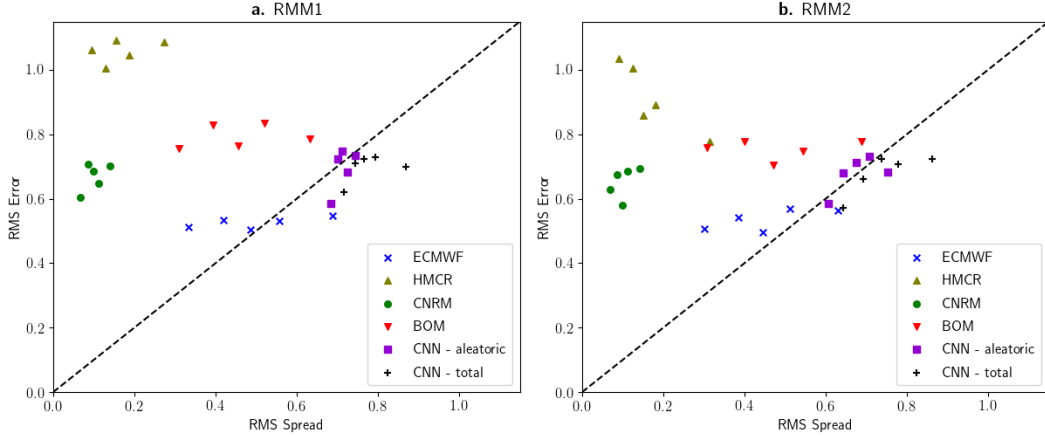


Figure 2. Error-Spread Diagrams for (a) RMM1 and (b) RMM2. Well calibrated forecasts lie on the one-to-one dashed line.

186 To quantify this property across many lead times, we incrementally remove the days
 187 with the highest predicted variance for each lead time and RMM index before comput-
 188 ing the RMSE in the forecast of the remaining days. This produces the confidence curve
 189 (Scalia et al., 2019). If the forecast correctly ranks different days in terms of forecast un-
 190 certainty, the confidence curve should be strictly decreasing. The error-drop (Figure 1(f)),
 191 is the ratio between the last and first points on the confidence curve (Scalia et al., 2019).
 192 The smaller the error-drop, the greater the reduction in RMSE when test days are sorted
 193 by the forecast uncertainty. The CNN performs better than all dynamical models. It is
 194 able to distinguish between predictable and unpredictable days at all lead times.

195 3.2 Interpretation to validate network behaviour

196 Before using the CNN to understand sources of uncertainty in the evolution of the
 197 MJO, we must understand how the CNN can make skilful forecasts of the MJO. This
 198 is necessary, as it reveals any concerning behaviour or spurious correlations (e.g. Lapuschkin
 199 et al., 2019), lending confidence to the predictions.

200 To interpret the CNN mean forecasts, we use the PatternNet algorithm (Kindermans
201 et al., 2017) to derive signal maps for each forecast. These indicate where information
202 is detected by the CNN in each input field. Because the different input variables are in-
203 troduced as separate channels into the CNN, weights are shared across all variables for
204 much of the network: the CNN distinguishes between variables in the first layer only. It
205 is therefore useful to consider both the signal maps averaged over all variables (the *sig-
206 nal mean*) and the difference between the signal map for each variable and the signal mean
207 map (the *signal anomalies*).

208 Since propagation over the Maritime Continent is a source of error in MJO fore-
209 casts in many models (Kim et al., 2016), we contrast one event which successfully prop-
210 agated over the Maritime Continent (28/02/2012), and one which decayed (25/02/2006)
211 to validate the CNN’s behaviour. Supporting Figure S1 shows the observed RMM in-
212 dices for these two events, and the corresponding mean forecasts initialised in phase 3,
213 which capture the observed behaviour.

214 Figure 3(a–b) shows the SHUM400 input fields averaged over all days in RMM
215 phase 3 for the decaying and the propagating events respectively. Panels (c–d) show the
216 signal means for RMM1 for the associated ten-day CNN forecasts initialised in phase 3.
217 (The signal means for the decaying RMM2 are much smaller, consistent with the pre-
218 diction that day-10 RMM2 is close to zero on average for the events selected: see Sup-
219 porting Figure S3). For both events, the CNN signal mean maps show that the CNN in-
220 tegrates over a large region spanning the Indian and Pacific Oceans, rather than tightly
221 focusing on the active MJO region: the CNN also derives information from the input fields
222 in regions of suppressed convection (Feng et al., 2015; Barrett et al., 2021).

223 Figure 3 (e–f) show the corresponding PatternNet signal anomalies for SHUM400,
224 highlighting the relative information provided by this input field. We see a large reduc-
225 tion in signal over the Pacific (150°E–90°W), and an enhancement over the Maritime Con-
226 tinent (90°E–110°E) co-located with enhanced SHUM400. Supporting Figures S4–S5 show
227 the equivalent figure for OLR. The RMM1 signal anomaly is greater than for SHUM400,
228 and it is stronger over the Pacific than was the case for SHUM400. Both Feng et al. (2015)
229 and Barrett et al. (2021) found OLR precursors in this region which distinguished be-
230 tween propagating and non-propagating MJO events. We conclude that the CNN has

231 identified true predictive features of MJO propagation, giving us confidence in the net-
 232 work.

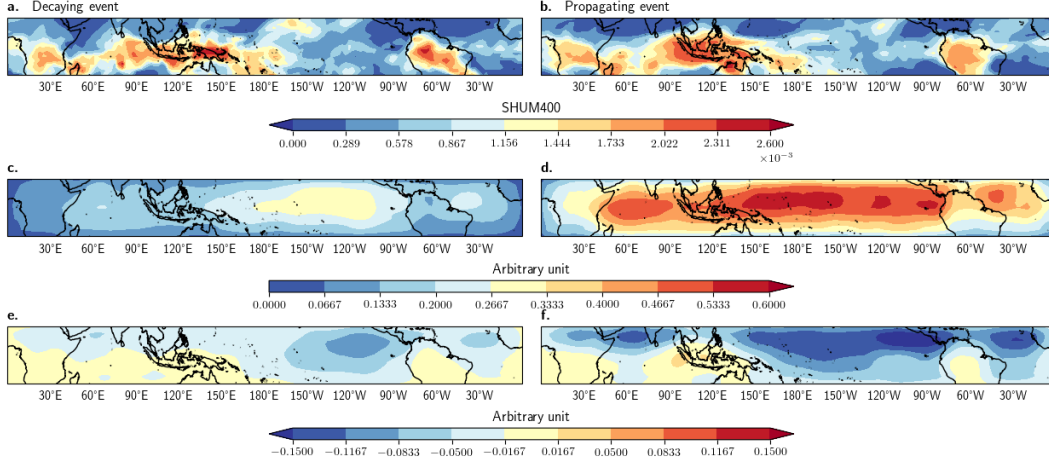


Figure 3. Interpretation of the CNN mean forecasts. (a–b) Composite maps of phase-3 SHUM400 for an MJO event which (a) decays and (b) propagates over the Maritime Continent. (c–d) PatternNet RMM1 signal mean maps (averaged over all variables) for ten-day CNN forecasts for the decaying and propagating event respectively. (e–f) RMM1 signal anomalies in SHUM400 for the decaying and propagating events respectively.

233 **3.3 Predictors of uncertainty in MJO forecasts**

234 The ability of the CNN to rank days by uncertainty enables us to investigate drivers
 235 of short-term predictability of the MJO. We consider cases in Boreal winter, and sep-
 236 arate MJO events into 4 categories according to the CNN’s 10-day forecast. We first cat-
 237 egorise according to strength: for each day, an event is weak (strong) if the initial ob-
 238 served RMM amplitude is less than (greater than) 1.0. The data are then divided into
 239 certain and uncertain forecasts. To study the uncertainty that is directly linked to the
 240 MJO initial conditions, we use the network’s predicted aleatoric uncertainty. An event
 241 is certain (uncertain) if both the RMM1 and RMM2 forecast aleatoric uncertainties are
 242 under (over) their respective 30% (70%) percentiles. For each initial observed phase and
 243 input feature, we compute the difference between certain and uncertain days, separately
 244 for weak and strong events.

245 Figure 4 shows the results for SHUM400 for events starting in phases 3 and 7. The
246 difference maps for weak and strong events are similar to each other: these maps pro-
247 vide information concerning factors influencing the uncertainty of the MJO forecasts as
248 opposed to its initial strength.

249 For MJO events in phase 3, the initial conditions of ‘certain’ forecasts have reduced
250 humidity at the equator in the central Pacific (150°E-120°W) and Indian Ocean (45°E-
251 100°E), combined with off-equatorial regions of enhanced humidity over the Maritime
252 Continent and Australia (100°E-160°E). Such a structure has been found to hinder the
253 eastward propagation of the MJO (Jiang et al., 2020). Looking at the outcome for each
254 type of event, we find $\sim 65\%$ of events classified as ‘certain’ are forecast weak by day-
255 10. In contrast, $\sim 80\%$ of ‘uncertain’ events are strong at day-10 (see Supporting Ta-
256 ble S3). This correlation between forecast strength at day-10 and forecast uncertainty
257 means one cannot draw conclusions as to whether the initial condition humidity anomaly
258 is a predictor of forecast strength, uncertainty, or both. To remove this confounding fac-
259 tor, we further stratified the events by strength at day-10. We found that the moisture
260 signal was substantially muted if we removed all events forecast as weak at day-10 from
261 the composites, whereas if only events forecast as transitioning from strong to weak were
262 considered, the signal became more intense (not shown). This confirms that final strength
263 is the dominant factor here.

264 For events initialised in phase 7, uncertain events show reduced moisture over the
265 Maritime Continent in the MJO suppressed region (90°E-120°E), and enhanced mois-
266 ture over the MJO active region (150°E-150°W), when compared to certain events. This
267 signature of an enhanced MJO signal in the initial conditions for unpredictable events
268 is observed for other variables for phase 7, particularly OLR (Supporting Figure S6). For
269 events initialised in phase 7, 85% of uncertain forecasts are also likely to be strong at
270 day-10, whereas that drops to 40% for certain forecasts (see Supporting Table S4). How-
271 ever, if we further stratify the forecasts by final strength, we find the signature persists
272 (not shown). Thus we conclude that an initially stronger MJO signal is associated with
273 more uncertainty in the forecast.

274 Finally, we find that MJO predictability is affected by the background state through
275 which it propagates. In particular, for certain events, Z850 shows an enhanced gradient
276 between the Eastern Pacific and the Maritime Continent for all forecasts initialised in

277 phases 4–7 (i.e. all events crossing the Pacific: see Supporting Figure S7–S8). An enhanced
 278 Z850 gradient is consistent with a higher Southern Oscillation index and a stronger Walker
 279 circulation cell over the Pacific. Further stratification by strength at day-10 indicates that
 280 this signal is unrelated to forecast strength. An enhanced (neutral or weakened) Walker
 281 circulation therefore leads to enhanced (reduced) certainty in the MJO.

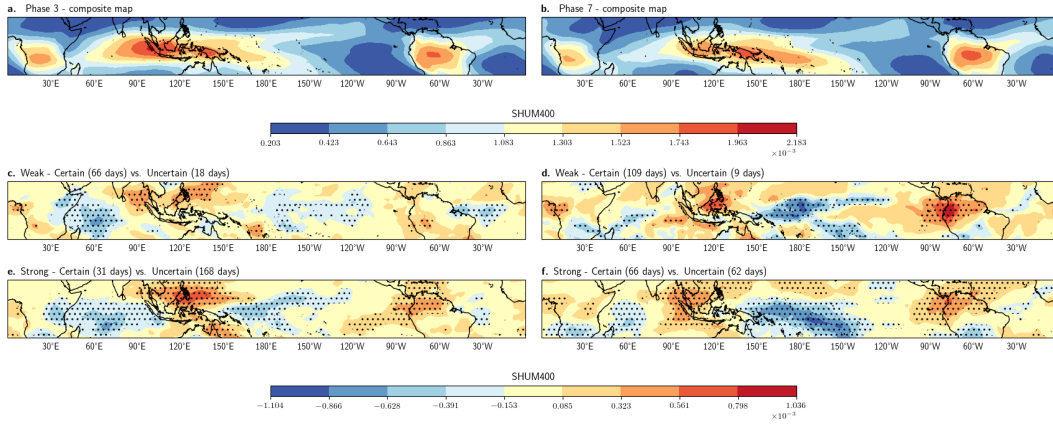


Figure 4. Interpretation of CNN uncertainty forecasts. (a-b) Composite maps of specific Humidity at 400hPa (SHUM400) for extended Boreal winter MJO events in (a) phase 3 and (b) phase 7. (c-f) Difference between input maps for predictable and unpredictable events as classified by ten-day forecasts using the CNN. (c) Weak phase 3 events (d) Weak phase 7 events. (e) Strong phase 3 events (f) Strong phase 7 events. Stippling denotes areas where anomalies are significant at the 95% level using the Student’s t-test.

282 4 Discussion and Conclusions

283 We presented a CNN framework which produces probabilistic forecasts of the MJO
 284 in terms of means and variances of the bivariate RMM index. The skill of the CNN is
 285 competitive with models from the S2S database. Moreover, the CNN outperforms all S2S
 286 models for one key forecast property: it can to rank start dates according to the fore-
 287 cast uncertainty associated with the initial conditions. In other words, the CNN fore-
 288 cast spread is a dynamic indicator of the uncertainty in the MJO forecast on a given day.

289 Since the CNN exhibits state-dependent reliability, we identify ‘certain’ CNN fore-
 290 casts with predictable states of the Earth system. We therefore interpret the CNN fore-
 291 casts to probe sources of predictability for the MJO. We do this by considering compos-

292 ites of initial conditions which the CNN indicated led to ‘certain’ and ‘uncertain’ ten-
293 day forecasts respectively. We found that for forecasts initialised in phase 3, reduced hu-
294 midity on the equator increases the likelihood of a decaying MJO event, which is asso-
295 ciated with high forecast certainty. However, enhanced humidity on the equator increases
296 the likelihood of MJO propagation over the MC, but it does not guarantee propagation,
297 leading to high uncertainty in the forecast and low medium-range predictability.

298 The CNN also used background state information to determine the MJO’s instan-
299 taneous predictability. A reduced gradient in Z850 was linked to more forecast uncer-
300 tainty for all MJO phases approaching the Pacific. This change in Z850 reflects a weaker
301 Walker circulation, associated with El-Niño events. However, we found no consistent sig-
302 nal in East Pacific SST across these phases (see Supporting Figures S9-S10). There is
303 substantial debate about the dependency of the MJO on the state of the El Niño-Southern
304 Oscillation (ENSO) (e.g. Ling et al., 2017). The Eastward extent of MJO activity is greater
305 in El Niño years, (Kessler, 2001), and the MJO lifetime and propagation speed is also
306 modulated by ENSO, though it shows sensitivity to the season of interest and type of
307 ENSO event (Pohl & Matthew, 2007; Pang et al., 2016). In contrast, the overall ampli-
308 tude of MJO activity appears unrelated to ENSO (J. M. Slingo et al., 1999; Kessler, 2001).
309 While the dependency of the MJO on the back-ground state is usually considered in terms
310 of SST, our results demonstrate ENSO could primarily influence the MJO via changes
311 to the atmospheric dynamical background associated with El Niño and La Niña.

312 Our CNN approach is complementary to earlier MJO predictability studies (e.g.
313 Neena et al., 2014; Wu et al., 2016; Kim et al., 2018). Instead of quantifying the poten-
314 tial predictability *limit* using our model, we are assessing relative predictability in the
315 medium-range across different initial conditions. We can only do this because the CNN
316 produces state dependent reliable probabilistic forecasts.

317 The CNN is competitive with the best available dynamical models at predicting
318 the MJO. However CNNs are complementary to dynamical models, and further improve-
319 ments to MJO forecasting may be achieved through a blend of dynamical and machine
320 learning approaches (Kim et al., 2021). Nevertheless, developing a stand-alone CNN fa-
321 cilitates interpretation, enabling us to probe the performance of the CNN and develop
322 new physical understanding, e.g. the role of different input features. This framework of
323 combining state-dependent uncertainty estimates from neural networks with interpre-

324 tation techniques could be applied to other climate phenomena, allowing us to quantify
 325 the diverse range of sources of uncertainty in the Earth System.

326 5 Open Research

327 Data related to this paper can be downloaded from ERA5 Copernicus database <https://>
 328 cds.climate.copernicus.eu/cdsapp#!/dataset/reanalysis-era5-pressure-levels,
 329 <https://cds.climate.copernicus.eu/cdsapp#!/dataset/reanalysis-era5-single>
 330 [-levels](https://cds.climate.copernicus.eu/cdsapp#!/dataset/reanalysis-era5-single-levels) and the S2S Project <ftp://s2sidx:s2sidx@acquisition.ecmwf.int/RMMS>.
 331 The RMM indices were computed using the CLIVAR diagnostics package available at
 332 <https://www.ncl.ucar.edu/Applications/mjoclivar.shtml>. PyTorch (<https://www>
 333 [.pytorch.org](https://www.pytorch.org)) and DropBlock (<https://github.com/miguelvr/dropblock>) libraries
 334 were implemented to build and train the CNN model. PatternNet code was adapted from
 335 https://github.com/TNTLFreiburg/pytorch_patternnet. The codes used in the cur-
 336 rent analysis are available at <https://www.github.com/adelaunay3/>.

337 Acknowledgments

338 H.M.C. was funded by Natural Environment Research Council grant number NE/P018238/1.

339 References

- 340 Arcomano, T., Szunyogh, I., Pathak, J., Wikner, A., Hunt, B. R., & Ott, E. (2020).
 341 A machine learning-based global atmospheric forecast model. *Geophysical Re-*
 342 *search Letters*, *47*(9).
- 343 Barrett, B. S., Densmore, C. R., Ray, P., & Sanabia, E. R. (2021, March). Active
 344 and weakening MJO events in the Maritime Continent. *Climate Dynamics*.
- 345 Bauer, P., Thorpe, A., & Brunet, G. (2015, sep). The quiet revolution of numeri-
 346 cal weather prediction. *Nature*, *525*(7567), 47–55. Retrieved from <http://www>
 347 [.nature.com/doi/10.1038/nature14956](http://www.nature.com/doi/10.1038/nature14956)
- 348 Bjerregård, M. B., Møller, J. K., & Madsen, H. (2021, June). An introduction to
 349 multivariate probabilistic forecast evaluation. *Energy and AI*, *4*, 100058. Re-
 350 trieved 2021-06-17, from [https://linkinghub.elsevier.com/retrieve/pii/](https://linkinghub.elsevier.com/retrieve/pii/S2666546821000124)
 351 [S2666546821000124](https://linkinghub.elsevier.com/retrieve/pii/S2666546821000124) doi: 10.1016/j.egyai.2021.100058
- 352 Bolin, D., & Wallin, J. (2019). Local scale invariance and robustness of proper scor-
 353 ing rules. , 1–26. Retrieved from <http://arxiv.org/abs/1912.05642>

- 354 Cassou, C. (2008). Intraseasonal interaction between the Madden-Julian Oscillation
355 and the North Atlantic Oscillation. *Nature*, *455*(7212), 523–527.
- 356 Christensen, H. M., Moroz, I. M., & Palmer, T. N. (2015). Evaluation of ensemble
357 forecast uncertainty using a new proper score: Application to medium-range
358 and seasonal forecasts. *Quarterly Journal of the Royal Meteorological Society*,
359 *141*(687), 538–549. doi: 10.1002/qj.2375
- 360 F. Vitart et al. (2017, January). The Subseasonal to Seasonal (S2S) Prediction
361 Project Database. *Bulletin of the American Meteorological Society*, *98*(1), 163–
362 173. (<ftp://s2sidx:s2sidx@acquisition.ecmwf.int/RMMS>)
- 363 Feng, J., Li, T., & Zhu, W. (2015). Propagating and nonpropagating MJO events
364 over maritime continent. *Journal of Climate*, *28*(21), 8430–8449. doi: 10.1175/
365 JCLI-D-15-0085.1
- 366 Ferranti, L., Palmer, T., Molteni, F., & Klinker, E. (1990). Tropical-extratropical
367 interaction associated with the 30–60 day oscillation and its impact on medium
368 and extended range prediction. *Journal of Atmospheric Sciences*, *47*(18),
369 2177–2199.
- 370 Gal, Y. (2016). *Uncertainty in Deep Learning* (Unpublished doctoral dissertation).
371 Cambridge University.
- 372 Gal, Y., & Ghahramani, Z. (2016). Dropout as a bayesian approximation: Repre-
373 senting model uncertainty in deep learning. In *international conference on ma-
374 chine learning* (pp. 1050–1059).
- 375 Ghiasi, G., Lin, T.-Y., & Le, Q. V. (2018, October). DropBlock: A regulariza-
376 tion method for convolutional networks. *arXiv:1810.12890 [cs]*. (arXiv:
377 1810.12890)
- 378 H. Hersbach et al. (2018a). ERA5 hourly data on pressure levels from 1979 to
379 present. *Copernicus Climate Change Service (C3S) Climate Data Store (CDS)*.
380 (Accessed on 01-03-2021, <https://doi.org/10.24381/cds.bd0915c6>)
- 381 H. Hersbach et al. (2018b). ERA5 hourly data on single levels from 1979 to present.
382 *Copernicus Climate Change Service (C3S) Climate Data Store (CDS)*. (Ac-
383 cessed on 01-03-2021, <https://doi.org/10.24381/cds.adbb2d47>)
- 384 Ham, Y.-G., Kim, J.-H., & Luo, J.-J. (2019). Deep learning for multi-year enso fore-
385 casts. *Nature*, *573*(7775), 568–572.
- 386 Henderson, G. R., Barrett, B. S., & M. Lafleur, D. (2014). Arctic sea ice and the

- 387 Madden–Julian Oscillation (MJO). *Climate Dynamics*, *43*(7-8), 2185–2196.
- 388 Hersbach, H. (2000). Decomposition of the continuous ranked probability score for
389 ensemble prediction systems. *Weather and Forecasting*, *15*(5), 559–570. doi: 10
390 .1175/1520-0434(2000)015<0559:DOTCRP>2.0.CO;2
- 391 Hersbach, H., et al. (2020). The ERA5 global reanalysis. *Quarterly Journal of the*
392 *Royal Meteorological Society*, *146*(730), 1999–2049. doi: 10.1002/qj.3803
- 393 Huntingford, C., Jeffers, E. S., Bonsall, M. B., Christensen, H. M., Lees, T., & Yang,
394 H. (2019). Machine learning and artificial intelligence to aid climate change
395 research and preparedness. *Environmental Research Letters*, *14*(12). doi:
396 10.1088/1748-9326/ab4e55
- 397 Jiang, X., Maloney, E., & Su, H. (2020, December). Large-scale controls of propaga-
398 tion of the Madden-Julian Oscillation. *npj Climate and Atmospheric Science*,
399 *3*(1), 29.
- 400 Kessler, W. S. (2001). EOF representations of the Madden-Julian and its connec-
401 tion with ENSO. *Journal of Climate*, *14*(13), 3055–3061. doi: 10.1175/1520
402 -0442(2001)014<3055:EROTMJ>2.0.CO;2
- 403 Kim, H., Ham, Y. G., Joo, Y. S., & Son, S. W. (2021, December). Deep learning for
404 bias correction of MJO prediction. *Nature Communications*, *12*(1), 3087.
- 405 Kim, H., Kim, D., Vitart, F., Toma, V. E., Kug, J.-S., & Webster, P. J. (2016,
406 June). MJO Propagation across the Maritime Continent in the ECMWF
407 Ensemble Prediction System. *Journal of Climate*, *29*(11), 3973–3988.
- 408 Kim, H., Vitart, F., & Waliser, D. E. (2018, December). Prediction of the
409 Madden–Julian Oscillation: A Review. *Journal of Climate*, *31*(23), 9425–
410 9443. Retrieved from [https://journals.ametsoc.org/doi/10.1175/
411 JCLI-D-18-0210.1](https://journals.ametsoc.org/doi/10.1175/JCLI-D-18-0210.1) doi: 10.1175/JCLI-D-18-0210.1
- 412 Kindermans, P.-J., Schütt, K. T., Alber, M., Müller, K.-R., Erhan, D., Kim, B., &
413 Dähne, S. (2017, October). Learning how to explain neural networks: Pattern-
414 Net and PatternAttribution. *arXiv:1705.05598 [cs, stat]*. Retrieved 2021-05-18,
415 from <http://arxiv.org/abs/1705.05598> (arXiv: 1705.05598)
- 416 Lapuschkin, S., Wäldchen, S., Binder, A., Montavon, G., Samek, W., & Müller,
417 K. R. (2019). Unmasking Clever Hans predictors and assessing what
418 machines really learn. *Nature Communications*, *10*(1), 1–8. Retrieved
419 from <http://dx.doi.org/10.1038/s41467-019-08987-4> doi: 10.1038/

- 420 s41467-019-08987-4
- 421 Leutbecher, M., & Palmer, T. (2008, March). Ensemble forecasting. *Journal*
 422 *of Computational Physics*, *227*(7), 3515–3539. Retrieved 2021-05-27, from
 423 <https://linkinghub.elsevier.com/retrieve/pii/S0021999107000812>
 424 doi: 10.1016/j.jcp.2007.02.014
- 425 Li, X., Yin, M., Chen, X., Yang, M., Xia, F., Li, L., ... Zhang, C. (n.d.). Impacts
 426 of the Tropical Pacific–Indian Ocean Associated Mode on Madden–Julian
 427 Oscillation over the Maritime Continent in Boreal Winter. , 14.
- 428 Lim, Y., Son, S.-W., & Kim, D. (2018, May). MJO Prediction Skill of the
 429 Subseasonal-to-Seasonal Prediction Models. *Journal of Climate*, *31*(10),
 430 4075–4094. Retrieved 2021-05-05, from [http://journals.ametsoc.org/doi/](http://journals.ametsoc.org/doi/10.1175/JCLI-D-17-0545.1)
 431 [10.1175/JCLI-D-17-0545.1](http://journals.ametsoc.org/doi/10.1175/JCLI-D-17-0545.1) doi: 10.1175/JCLI-D-17-0545.1
- 432 Ling, J., Li, C., Li, T., Jia, X., Khouider, B., Maloney, E., ... Zhang, C. (2017).
 433 Challenges and opportunities in MJO studies. *Bulletin of the American Meteoro-*
 434 *logical Society*, *98*(2), ES53–ES56. doi: 10.1175/BAMS-D-16-0283.1
- 435 Madden, R. A., & Julian, P. R. (1971). Detection of a 40–50 day oscillation in the
 436 zonal wind in the Tropical Pacific. *Journal of the Atmospheric Sciences*, *28*,
 437 702–708. doi: 10.1017/CBO9781107415324.004
- 438 Marshall, A. G., Hendon, H. H., & Hudson, D. (2016). Visualizing and verifying
 439 probabilistic forecasts of the Madden-Julian Oscillation. *Geophysical Research*
 440 *Letters*, *43*(23), 12,278–12,286. doi: 10.1002/2016GL071423
- 441 Martin, Z., Barnes, E., & Maloney, E. (2021, March). *Predicting the MJO us-*
 442 *ing interpretable machine-learning models* (Tech. Rep.). Atmospheric Sci-
 443 ences. Retrieved 2021-04-01, from [http://www.essoar.org/doi/10.1002/](http://www.essoar.org/doi/10.1002/essoar.10506356.1)
 444 [essoar.10506356.1](http://www.essoar.org/doi/10.1002/essoar.10506356.1) doi: 10.1002/essoar.10506356.1
- 445 Neena, J. M., Lee, J. Y., Waliser, D., Wang, B., & Jiang, X. (2014). Predictabil-
 446 ity of the Madden-Julian oscillation in the Intraseasonal Variability Hind-
 447 cast Experiment (ISVHE). *Journal of Climate*, *27*(12), 4531–4543. doi:
 448 10.1175/JCLI-D-13-00624.1
- 449 Palmer, T. N. (2000). Predicting uncertainty in forecasts of weather and climate.
 450 *Reports on Progress in Physics*, *63*(2), 71–116. doi: 10.1088/0034-4885/63/2/
 451 201
- 452 Pang, B., Chen, Z., Wen, Z., & Lu, R. (2016). Impacts of two types of El Niño on

- 453 the MJO during boreal winter. *Advances in Atmospheric Sciences*, 33(8), 979–
454 986. doi: 10.1007/s00376-016-5272-2
- 455 Pohl, B., & Matthew, A. J. (2007). Observed changes in the lifetime and ampli-
456 tude of the Madden-Julian oscillation associated with interannual ENSO sea
457 surface temperature anomalies. *Journal of Climate*, 20(11), 2659–2674. doi:
458 10.1175/JCLI4230.1
- 459 Reichstein, M., Camps-Valls, G., Stevens, B., Jung, M., Denzler, J., Carval-
460 hais, N., & Prabhat. (2019). Deep learning and process understanding
461 for data-driven Earth system science. *Nature*, 566(7743), 195–204. Re-
462 trieved from <http://dx.doi.org/10.1038/s41586-019-0912-1> doi:
463 10.1038/s41586-019-0912-1
- 464 Roulston, M. S., & Smith, L. A. (2002). Evaluating probabilistic forecasts using in-
465 formation theory. *Monthly Weather Review*, 130(6), 1653–1660. doi: 10.1175/
466 1520-0493(2002)130(1653:EPFUIT)2.0.CO;2
- 467 Russakovsky, O., Deng, J., Su, H., Krause, J., Satheesh, S., Ma, S., . . . others
468 (2015). Imagenet large scale visual recognition challenge. *International journal*
469 *of computer vision*, 115(3), 211–252.
- 470 Scalia, G., Grambow, C. A., Pernici, B., Li, Y.-P., & Green, W. H. (2019, October).
471 Evaluating Scalable Uncertainty Estimation Methods for DNN-Based Molecu-
472 lar Property Prediction. *arXiv:1910.03127 [cs, stat]*. (arXiv: 1910.03127)
- 473 Schultz, M., Betancourt, C., Gong, B., Kleinert, F., Langguth, M., Leufen, L., . . .
474 Stadtler, S. (2021). Can deep learning beat numerical weather prediction?
475 *Philosophical Transactions of the Royal Society A*, 379(2194).
- 476 Slingo, J., & Palmer, T. (2011). Uncertainty in weather and climate prediction.
477 *Philosophical Transactions of the Royal Society A: Mathematical, Physical and*
478 *Engineering Sciences*, 369(1956), 4751–4767.
- 479 Slingo, J. M., Rowell, D. P., Sperber, K. R., & Nortley, F. (1999). On the pre-
480 dictability of the interannual behaviour of the Madden-Julian Oscillation and
481 its relationship with El Nino. *Quarterly Journal of the Royal Meteorological*
482 *Society*, 125(554), 583–609. doi: 10.1256/smsqj.55410
- 483 Toms, B. A., Kashinath, K., Prabhat, & Yang, D. (2020). Testing the reliabil-
484 ity of interpretable neural networks in geoscience using the madden-julian
485 oscillation. *Geoscientific Model Development Discussions*, 2020, 1–22. Re-

- 486 trieved from <https://gmd.copernicus.org/preprints/gmd-2020-152/> doi:
487 10.5194/gmd-2020-152
- 488 Translational Neurotechnology Lab. (2019). PatternNet GitHub Repository.
489 (University of Freiburg, [https://github.com/TNTLFreiburg/pytorch\
490 _patternnet](https://github.com/TNTLFreiburg/pytorch_patternnet))
- 491 Vitart, F. (2017, July). Madden—Julian Oscillation prediction and teleconnec-
492 tions in the S2S database. *Quarterly Journal of the Royal Meteorological Soci-
493 ety*, 143(706).
- 494 Vitart, F., & Robertson, A. W. (2018). The sub-seasonal to seasonal prediction
495 project (S2S) and the prediction of extreme events. *npj Climate and Atmo-
496 spheric Science*, 1(1), 1–7. Retrieved from [http://dx.doi.org/10.1038/
497 s41612-018-0013-0](http://dx.doi.org/10.1038/s41612-018-0013-0) doi: 10.1038/s41612-018-0013-0
- 498 Wheeler, M. C., & Hendon, H. H. (2004). An All-Season Real-Time Multivariate
499 MJO Index: Development of an Index for Monitoring and Prediction. *Monthly
500 Weather Review*, 132, 16.
- 501 Wu, J., Ren, H. L., Zuo, J., Zhao, C., Chen, L., & Li, Q. (2016). MJO predic-
502 tion skill, predictability, and teleconnection impacts in the Beijing Climate
503 Center Atmospheric General Circulation Model. *Dynamics of Atmospheres
504 and Oceans*, 75, 78–90. Retrieved from [http://dx.doi.org/10.1016/
505 j.dynatmoce.2016.06.001](http://dx.doi.org/10.1016/j.dynatmoce.2016.06.001) doi: 10.1016/j.dynatmoce.2016.06.001
- 506 Yoo, C., Lee, S., & Feldstein, S. B. (2012). Arctic response to an mjo-like tropi-
507 cal heating in an idealized gcm. *Journal of Atmospheric Sciences*, 69(8), 2379–
508 2393.
- 509 Zhang, C. (2013). Madden-Julian Oscillation: Bridging weather and climate. *Bul-
510 letin of the American Meteorological Society*, 94(12), 1849–1870. doi: 10.1175/
511 BAMS-D-12-00026.1